in C14 and the corresponding calculated results (solid lines) for various values of D_{eff}. The initial temperature T_i was set at 25 °C and the numerical results were obtained for $\tau = 6.0$ s, $q = 0.166$ nm^{-1}, and $\Delta H_a = 9.0$ kcal/mol, where τ was measured and q is the scattering vector at which the intensity change was measured. The activation energy ΔH_a was measured independently from the temperature dependence of D_{eff}'s, which, in turn, were measured from the slope of log $I(q,t;T_m)$ vs. t at $t \gg \tau$.

The numerical results for $D_{eff} \to \infty$ correspond to a fictitious case of infinitely large D_{eff} for which the intensity decrease with time is a mere consequence of a reduction of static intensity after a temperature increase as characterized by eq 3. The results for $D_{eff} \to \infty$ were uniquely determined by the change of static scattered intensity with temperature, $I_s(q;T)$, and the change of temperature with time, $T(t)$. The experimental evidence that the measured intensity decay with time is much slower than the decay predicated for $D_c \to \infty$ firmly confirms that the observed decay primarily reflects the molecular diffusion process.

The best fits yield the effective diffusivities of 1.8 ± 0.1 and 3.0 ± 0.1 nm^2/s at 150 and 170 °C, respectively. The results agree with those determined from the slopes of log $I(q,t;T_m)$ vs. t at $t \gg \tau$. The method involving the T-jump and time-resolved SAXS analyses now seems to be well established and useful for characterization of the kinetics and molecular dynamics of the order–disorder transition of block polymers in the time scale of as short as a few seconds. The intensity decay with time during the order–disorder transition reflects the effective diffusivity D_{eff}. The larger the value D_{eff}, the faster the rate of the intensity decay. Further quantitative studies will be presented in a subsequent paper[12] on the kinetics of the order–disorder transition as a function of temperature and concentration.

References and Notes

(1) Leibler, L. *Macromolecules* **1980**, *13*, 1602.
(2) Roe, R. J.; Fishkis, M.; Chang, J. C. *Macromolecules* **1981**, *14*, 1091.
(3) Hashimoto, T.; Shibayama, M.; Kawai, H. *Polym. Prepr., Am. Chem. Soc. Div. Polym. Chem.* **1982**, *23* (1), 21.
(4) Hashimoto, T.; Shibayama, M.; Kawai, H. *Macromolecules* **1983**, *16*, 1093.
(5) Hashimoto, T.; Tsukahara, Y.; Kawai, H. *Polym. J.* **1983**, *15*, 699.
(6) Mori, K.; Hasegawa, H.; Hashimoto, T. *Polym. J.* **1985**, *17*, 799.
(7) Bates, F. S. *Macromolecules* **1985**, *18*, 525.
(8) Hashimoto, T.; Tsukahara, Y.; Kawai, H. *J. Polym. Sci., Polym. Lett. Ed.* **1980**, *18*, 585; *Macromolecules* **1981**, *14*, 708.
(9) Hashimoto, T.; Suehiro, S.; Shibayama, M.; Saijo, K.; Kawai, H. *Polym. J.* **1981**, *13*, 501.
(10) Hashimoto, T.; Shibayama, M.; Kowsaka, K., to be submitted to *Macromolecules* (part 3 of this series).
(11) Shibayama, M.; Hashimoto, T.; Kawai, H. *Macromolecules* **1983**, *16*, 16.
(12) Hashimoto, T.; Kowsaka, K.; Shibayama, M.; Kawai, H. *Macromolecules* **1986**, *19*, 754.
(13) de Gennes, P.-G. "Scaling Concepts in Polymer Physics"; Cornell University Press: Ithaca, NY, 1979.
(14) LeGrand, A. D.; LeGrand, D. G. *Macromolecules* **1979**, *12*, 450.
(15) Leibler, L.; Benoit, H. *Polymer* **1981**, *22*, 195.
(16) Benmouna, M.; Benoit, H. *J. Polym. Sci., Polym. Phys. Ed.* **1983**, *21*, 1227.
(17) We assume here that ΔH_a does not change below and above T_r. It should be noted that Chung and Lin[18] reported a discontinuity in ΔH_a for a viscous flow of SBS block polymer in the bulk around T_r, obtaining 22.8 and 19.4 kcal/mol below and above T_r, respectively. A similar discontinuity might apply to ΔH_a in our system. In our case the solvent may reduce the value of ΔH_a and hence the difference of ΔH_a below and above T_r.
(18) Chung, C. I.; Lin, M. I. *J. Polym. Sci., Polym. Phys. Ed.* **1978**, *16*, 545.

Time-Resolved Small-Angle X-ray Scattering Studies on the Kinetics of the Order–Disorder Transition of Block Polymers. 2. Concentration and Temperature Dependence

Takeji Hashimoto,* Keisuke Kowsaka,† Mitsuhiro Shibayama,‡ and Hiromichi Kawai§

Department of Polymer Chemistry, Faculty of Engineering, Kyoto University, Kyoto 606, Japan.

Received June 25, 1985

ABSTRACT: Equilibrium and kinetic aspects of the order–disorder transition of polystyrene–polybutadiene diblock polymer solutions in *n*-tetradecane were studied as a function of polymer concentration and temperature by small-angle X-ray scattering (SAXS). The order–disorder transition temperature (T_r) was determined by analyzing thermal concentration fluctuations of polystyrene and polybutadiene segments as a function of temperature in the disordered state. The kinetics were studied by time-resolved measurements of SAXS profiles on the time scale of a few seconds during the order–disorder transition after a temperature jump above T_r. The kinetic studies gave estimations of the translational diffusivities D_{eff} for the center-of-mass motion of the block polymers in the solutions and the activation energies for the diffusion process. The activation energies determined by the SAXS technique were found to be in good agreement with those determined from rheological measurements.

I. Introduction

In this paper we investigate the temperature T_r and kinetics of the order–disorder transition of polystyrene–polybutadiene diblock polymers (SB) in *n*-tetradecane (C14) using small-angle X-ray scattering (SAXS). The transition temperature was determined as a function of polymer concentration by analyzing SAXS arising from thermal concentration fluctuations of polystyrene (PS) and polybutadiene (PB) segments in the disordered state[1-3] (i.e., the state where PS and PB block chains are molecularly mixed) as a function of temperature (section IV). The theoretical background for the scattering from block polymers in the disordered state may be found in the work of de Gennes,[4] LeGrand and LeGrand,[5] Leibler,[1,6] and Benoit and Benmouna.[7]

The kinetics of the order–disorder transition was studied

† Present address: Textile Research Laboratory, Asahi Chemical Industry Co., Ltd., Takatsuki, Osaka 569, Japan.
‡ Present address: Department of Polymer Science and Engineering, Kyoto Institute of Technology, Matsugasaki, Kyoto 606, Japan.
§ Present address: Hyogo University of Education, Yashiro-cho, Kato-gun, Hyogo-ken, Japan.

0024-9297/86/2219-0754$01.50/0

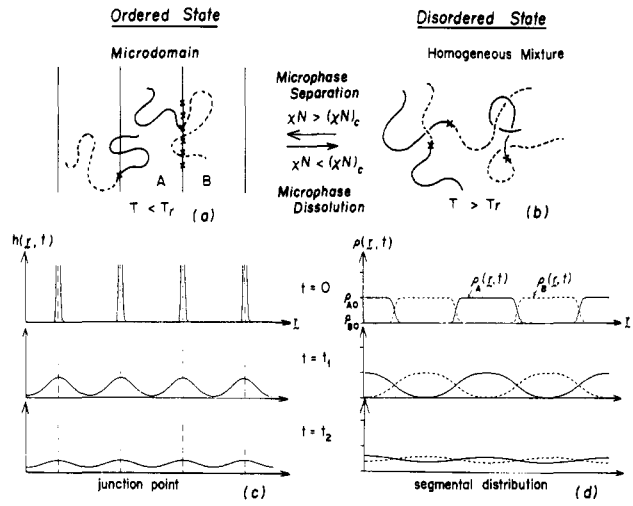

Figure 1. Schematic diagrams showing the ordered state (a) and disordered state (b) of block polymers and the change of spatial distribution of the chemical junctions $h(\mathbf{r},t)$ (c) and segmental density profile $\rho_K(\mathbf{r},t)$ (d) with time during the order–disorder transition (i.e., microphase dissolution).

by using the time-resolved SAXS method coupled with temperature-jump (T-jump) technique as described in detail in part 1 of this series.[8] The theoretical background is briefly reviewed in section III, and the results and discussion are presented in section V. Equilibrium aspects of the transition are discussed in section IV. In section VI we discuss the change in rheological behavior accompanying the order–disorder transition (i.e., from non-Newtonian flow to Newtonian flow) and compare the activation energy estimated from rheological behavior in the disordered state with that estimated from the kinetic studies.

II. Experimental Methods

A commercial SB block polymer (Phillips Petroleum, Solprene 1205) was used as received without further purification. The polymer has a number-average molecular weight $M_n = 5.2 \times 10^4$ as determined by membrane osmometry and a weight fraction of PS $W_{PS} = 0.30$ as determined by elemental analysis. The solutions studied are n-tetradecane solutions (coded as C14). The solvent is not volatile and is selectively good for PB but poor for PS, the solubility parameters for PS, PB, and C14 being 9.1, 8.4, and 7.8 cal/cm^3.

The solutions were prepared by mixing prescribed amounts of SB and an excess of methylene chloride, a good solvent for both PB and PS, which was subsequently evaporated completely to obtain a homogeneous solution of a given concentration. The polymer concentration range covered was from 15.0 to 40.0 wt %.

The SAXS apparatus, time-resolved SAXS technique, and temperature-jump method were described in detail in part 1 of this series.[8]

III. Theoretical Background on Kinetics of Order–Disorder Transition

The principles of the kinetics of the order–disorder transition were described in an earlier paper.[9] Here we briefly review the principle and add some discussion and remarks.

Figure 1 schematically presents the order–disorder transition (a, b) for A–B diblock polymers and the molecular process of the transition (c, d). In the ordered state (a), the (repulsive) energetic interactions between polymers A and B outweigh the entropy effects, resulting in segregation of polymers A and B in their respective microdomains and in spatial confinement of chemical junctions of A and B in the block polymers in the narrow interfacial region (Figure 1a). In the disordered state, on the other hand, the entropy effects outweigh the energetics, resulting in random placement of the chemical junctions in space and in molecular mixing (Figure 1b).

The order–disorder transition is a thermally reversible process. In the context of the mean-field approximation, the transition point is a function of fraction f_A of one polymer component, e.g., A, and χN_s, where χ is the thermodynamic interaction parameter between A and B and N is the total degree of polymerization.

$$f_A = N_A/(N_A + N_B) \quad (1)$$

$$N = N_A + N_B \quad (2)$$

N_K (K = A or B) is the degree of polymerization of the K block of the copolymer chain. For a given block polymer with a given f_A, microphase separation occurs if $\chi N > (\chi N)_c$, and microphase dissolution occurs if $\chi N < (\chi N)_c$, where $(\chi N)_c$ determines the transition point.[1] For polymer pairs having dispersive interactions only, as in PS and PB, microphase dissolution (separation) takes place by increasing (decreasing) temperature above (below) T_r.

When the thermodynamic driving force stabilizing the microdomains is removed suddenly by a temperature jump to a temperature above T_r, energy-driven center-of-mass motions of block polymers occur, giving rise to a broader spatial distribution of the chemical junctions $h(\mathbf{r},t)$ with time (Figure 1c). The diffusion of polymer molecules in entangled melts or concentrated solutions may take place through reptation, the curvilinear diffusion of a chain molecule along its own contour as discussed by de Gennes[10] and Doi and Edwards.[11] As reptation proceeds, the junctions and the segments lose their memories with respect to their positions in space, giving rise to a broader distribution of $h(\mathbf{r},t)$ and to a change of spatial segmental distribution $\rho_K(\mathbf{r},t)$ (K = A or B) with time (Figure 1d). As time goes on, the interfacial thickness increases and the segmental intermixing further progresses, resulting in eventually a homogeneous segmental density profile characteristic of the disordered state.

If the temperature is raised sufficiently high above T_r, the thermodynamic interaction between A and B does not significantly affect the diffusional flow. Under this condition, the change of the segmental density profile caused by the thermal motion of the molecules is given by

$$\partial\rho_K(\mathbf{r},t)/\partial t = D_c\nabla^2\rho_K(\mathbf{r},t) \quad (K = A \text{ or } B) \quad (3)$$

where D_c is the diffusivity for the center of mass of the block polymer as a whole. $\rho_K(\mathbf{r},t)$ denotes the reduced density of monomers K, defined as the ratio of the local density of monomers K at point $\mathbf{r}$ and time t to the overall monomer density averaged over the sample.

$$\rho_A(\mathbf{r},t) + \rho_B(\mathbf{r},t) = 1 \quad (4)$$

When the thermodynamic interaction affects the diffusional flow, D_c should be modified by an effective diffusivity D_{eff}

$$\partial\rho_K(\mathbf{r},t)/\partial t = D_{eff}\nabla^2\rho_K(\mathbf{r},t) \quad (K = A \text{ or } B) \quad (5)$$

where D_{eff} should depend on χ as well as on the frictional interactions. Equation 5 is derived for the dissolution of the concentration fluctuations in a polymer mixture in the Appendix.

Solving eq 5 under appropriate, periodic, initial conditions relevant to the microdomain systems $\rho_{K,j}(\mathbf{r},t=0)$ as shown in Figure 1c,d at $t = 0$, one obtains

$$\rho_{K,j}(\mathbf{r},t) = \rho_{K,j}(\mathbf{r},t=0)*h_j(\mathbf{r},t) \quad (K = A \text{ or } B) \quad (6)$$

where the asterisk denotes the convolution product, j denotes the dimensionality (j = 1–3), $\rho_{K,j}(\mathbf{r},t=0)$ is the

initial segmental density profile, and $h_j(\mathbf{r},t)$ is the change of the spatial distribution of the chemical junctions with time, which is obtained by solving eq 5

$$h_j(\mathbf{r},t) = \left(\frac{j}{2\pi\sigma_j^2}\right)^{j/2} \exp\left\{-\frac{jr^2}{2\sigma_j^2}\right\} \tag{7}$$

$$\sigma_j^2 = \sigma_{0j}^2 + 2jD_{\text{eff}}t \qquad (j = 1\text{–}3) \tag{8}$$

where σ_{0j} is the standard deviation of $h_j(\mathbf{r},t=0)$, the initial spatial distribution of the chemical junctions as shown in Figure 1c at $t = 0$. The standard deviation $\sigma_j(t)$ predicts a change of the characteristic interfacial thickness $\xi(t)$ during the dissolution process[9]

$$\xi(t)^{-1} = |\partial\rho_K(\mathbf{r},t)/\partial r|_{\rho_K=\rho_{K0}/2} \tag{9}$$

and

$$\xi(t) = [2\pi(\sigma_0^2 + 2D_{\text{eff}}t)]^{1/2} \tag{10}$$

The dimensionality j is related to the dimensionality of the segmental density profile. For example, the alternating lamellar microdomain system shown in Figure 1a has one-dimensional fluctuations in the segmental density profile $\rho_K(\mathbf{r},t)$ and hence corresponds to $j = 1$. Similarly, the cylindrical and spherical microdomain systems correspond to the case of $j = 2$ and 3, respectively.

Accompanying the change of the segmental density profile with time as given by eq 6–8, the elastic scattered intensity profile $I(q,t)$ changes with time during the order–disorder transition in the following manner:

$$I(q,t) = I(q,t=0) \exp[-2R(q)t] \tag{11}$$

where

$$R(q) = q^2D_{\text{eff}} \tag{12}$$

irrespective of the dimensionality,[9] $I(q,t=0)$ is the initial scattered intensity profile, and q is the scattering vector as defined by

$$q = 2\pi s$$
$$s = (2/\lambda) \sin\theta \tag{13}$$

where λ is the wavelength of radiation in the medium and 2θ is the scattering angle in the medium. The elastic scattered intensity decays exponentially with time at a rate $2R(q)$ which is proportional to q^2 and D_{eff}.

Figure 2 shows computer simulations of changes of the segmental density profiles $\rho_A(Z/D,t)$ with time and the corresponding change of the elastic scattered intensity profiles log $[I(sD,t)/NI_e]$ with time during the dissolution of the lamellar microdomain. Here, Z is the distance normal to the interface. All the calculated intensity profiles are those along the direction normal to the lamellar interfaces. It should be noted that $\rho_B(Z/D,t)$ should change with time, although not shown in Figure 2, in such a manner that it satisfies

$$\rho_A(Z/D,t) + \rho_B(Z/D,t) = 1 \tag{14}$$

where D is the average identity period of the alternating lamellar microdomain. The simulations were made for the perfectly oriented one-dimensional assembly of lamellae[18] under the following conditions: (i) the volume fraction of one type of lamella f is 0.5, resulting in extinction of the even-order scattering maxima at $sD = 2m$ (m = integer), (ii) standard deviations of the domain identity period ΔD and that of the thickness of the A and B lamellae ΔL from the average value ΔL are assumed to satisfy $\Delta D/D = \Delta L/L = 0.05$, and (iii) the average number of lamellar pairs in the assembly N is 10 and the standard deviation ΔN of the number from N is 3.0 (the condition affecting only the zero-order scattering). The σ value in the figure corresponds to σ_1 in eq 8, which describes changes of the segmental density profiles and scattered intensity profiles with time. The intensity profiles were calculated according to Hosemann's paracrystal theory of scattering[12] and the detailed procedure is described elsewhere.[19] The intensity I_e is the Thomson scattering intensity.

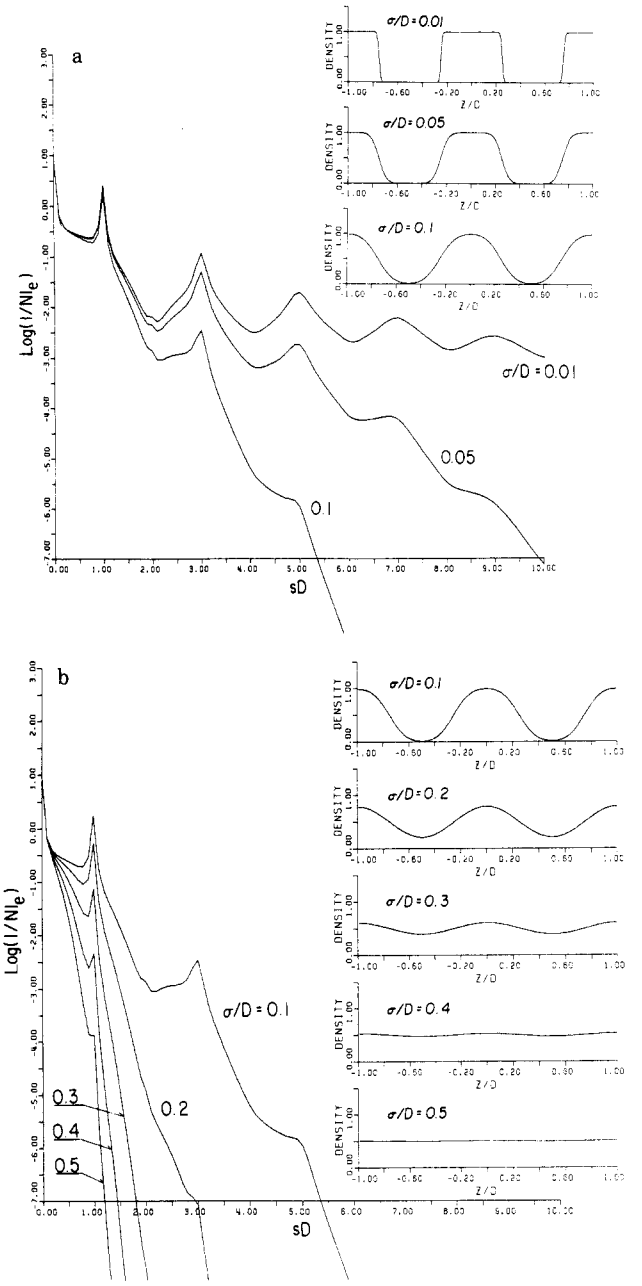

Figure 2. Computer simulations of the change of the segmental density profile of one type of domain, e.g., the A microdomain, and the elastic scattered intensity profile I/NI_e with time during the order–disorder transition. The simulations were performed for alternating lamellar microdomains with volume fraction of one type of domain $f_A = 0.5$. D is the domain identity period and σ is the standard deviation of $h(\mathbf{r},t)$, which increases with time ($\sigma^2 \equiv \sigma_1^2 = \sigma_{01}^2 + 2D_{\text{eff}}t$) for the lamellar microdomain. The scattering profiles were calculated on the basis of the paracrystal model described in the text, and the even-order maxima are not seen due to the extinction effect.

As dissolution proceeds, the value σ increases, which involves increasing interfacial thickness $\xi(t)$ and increasing segmental intermixing. In correspondence to the change of the segmental density profile, the scattered intensity decreases with increasing σ/D. The rate of the intensity

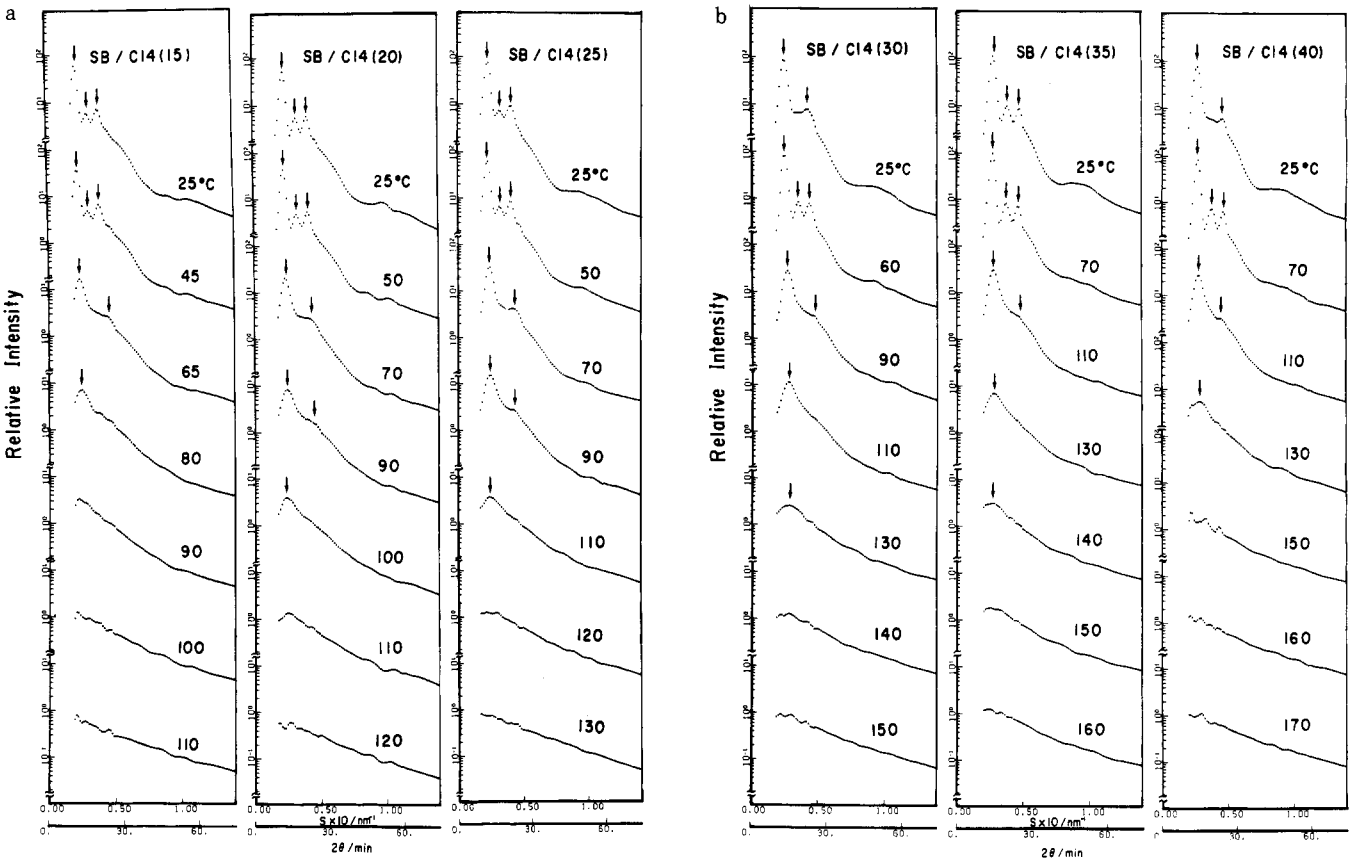

Figure 3. Change of static scattered intensity with temperature for SB solutions with various concentrations. Logarithm of relative scattered intensity was plotted as a function of s nm^{-1} or 2θ min.

decay is faster for larger sD or q, satisfying eq 11 and 12.

IV. Order-Disorder Transition Temperature

Figure 3 shows static SAXS profiles (logarithm of intensity vs. s) at various temperatures for the solutions studied in this work. The detailed analyses of the profiles at low temperatures were presented in the previous paper.[13,14] At low temperatures, PS block chains segregate into spherical microdomains. The spherical domains are dispersed in the matrix of PB solutions and are arranged in space with a long-range order as characterized by a superlattice having a simple-cubic-like symmetry. The superlattice was found to be stabilized by the entropy elasticity of the confined chains.[14] The scattering maxima marked by arrows, which are located at relative angular positions of $1:2^{1/2}:3^{1/2}$ to the first-order peak position, can be attributed to the interference of the scattering waves from the domains in the superlattice. As temperature goes up the lattice disordering takes place, which results in broadening of the scattering maxima.[14]

The microdomains themselves are dissolved into a disordered solution corresponding to the state shown in Figure 1b at still higher temperature (above the order-disorder transition temperature T_r). It should be noted, however, that the disordered solution still exhibits a single scattering maximum which is much broader and weak compared with the first-order maximum from the microdomains. This maximum is called the maximum from the correlation hole.[4] This maximum is interpreted to be a consequence of the fact that the connectivity between PS and PB in SB diblock polymers invokes the wavelengths of particular Fourier components of the thermal concentration fluctuations which give rise to the maximum amplitude of the fluctuations. Close observation of the profiles shown in Figure 3 indicates existence of the broad and weak scattering maximum even at temperatures higher than T_r (see Table I). Plots of the profiles on a linear intensity scale more clearly show the scattering maximum. The temperature T_r may be qualitatively determined as the temperature above which the higher order interference maxima become indistinguishable. A more quantitative method to determine T_r is presented below.

Table I
Order-Disorder Transition Temperature T_r of SB Solutions with C14 as a Function of Polymer Concentration

c, wt %	15.0	20.0	25.0	30.0	35.0	40.0
T_r, °C	85 ± 5	95 ± 5	105 ± 5	110 ± 5	120 ± 5	125 ± 5

Leibler presented a scattering theory for bulk block polymers in the disordered state in the context of the random phase approximation.[1] According to the theory, the scattered intensity $I(q)$ is given by

$$I(q) \sim N/[F(u) - \chi N] \tag{15}$$

where $F(u)$ is given by eq IV-6 of ref 1 and u is defined as

$$u = qR_0 \tag{16}$$

R_0 is the radius of gyration of the block polymer chain in the unperturbed state. We may extend Leibler's theory to concentrated block polymer solutions in the disordered state by replacing χ by χ_{eff}

$$\chi_{eff} = \chi\phi_p \tag{17}$$

where ϕ_p is the volume fraction of polymer in solution and χ is the thermodynamic interaction parameter between the constituent polymers in the bulk.[15] The variable u should be replaced by u'

$$u' = qR$$

where R is the radius of gyration of the polymer in the solution.

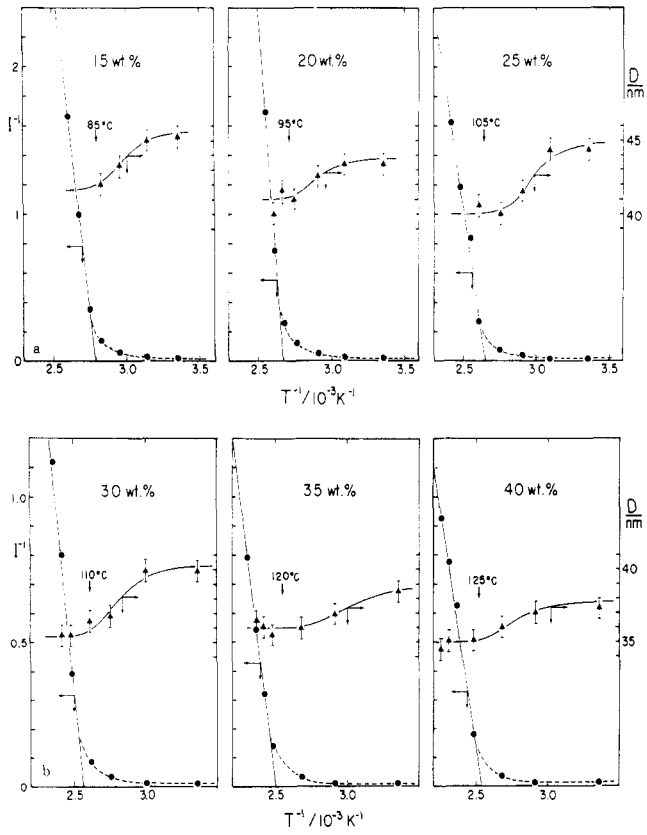

Figure 4. Reciprocal scattered intensity I^{-1} at a given q near q_m and the apparent Bragg spacing D as determined from the first-order maximum as a function of T^{-1} for SB solutions with various concentrations.

The approximation of eq 17 should be good for nonselective solvents but may be less satisfactory for selective solvents such as C14. Despite this fact we use here the approximation of eq 17 for further semiquantitative analyses of the order–disorder transition. More rigorous analyses may be carried out by using the theory presented by Benmouna and Benoit[7] for the block polymer solutions in the disordered state. However, this is beyond the scope of the present paper. If χ is written as

$$\chi = A + B/T \tag{18}$$

then from eq 15 and 18

$$I(q)^{-1} \sim \left(\frac{F(u')}{N\phi_p} - A \right) - B/T \tag{19}$$

Hence in the disordered state I^{-1} should decrease linearly with T^{-1}. Equation 15 also predicts that the scattering maximum occurs at $u = u_{max}$, where $F(u) - \chi N$ becomes minimum; i.e.

$$u_{max} = q_{max} R_0 \tag{20}$$

Thus the scattering vector q_{max} giving rise to the maximum intensity should be independent of temperature T since R_0 is not a sensitive function of T. The q_{max} for the solutions should also be independent of T since R is also not sensitive to T. The concentration dependence of q_{max} should reflect the concentration dependence of R.

Figure 4 shows the analyses of the order–disorder transition based on eq 19. The D values are apparent Bragg spacings estimated from

$$D = 2\pi/q_{max} \tag{21}$$

At sufficiently high temperatures, I^{-1} decreases linearly with T^{-1}, and D is independent of T, indicating that the block polymer solutions are in the disordered state in this temperature range. Upon lowering temperature, the deviation from the linearity of I^{-1} with T^{-1} and the increase of D with T start to occur at nearly the same temperature T_r for a given solution. The deviation from the linearity and the increase of D are considered to be consequences of the onset of microphase separation, and this temperature T_r corresponds to the temperature at which the order–disorder transition occurs. Thus D has different physical meaning above and below T_r: (i) in the disordered state D corresponds to the wavelength of the particular Fourier components of thermal concentration fluctuations which have maximum amplitude of fluctuations and (ii) in the ordered state it corresponds to the identity period of the domains.

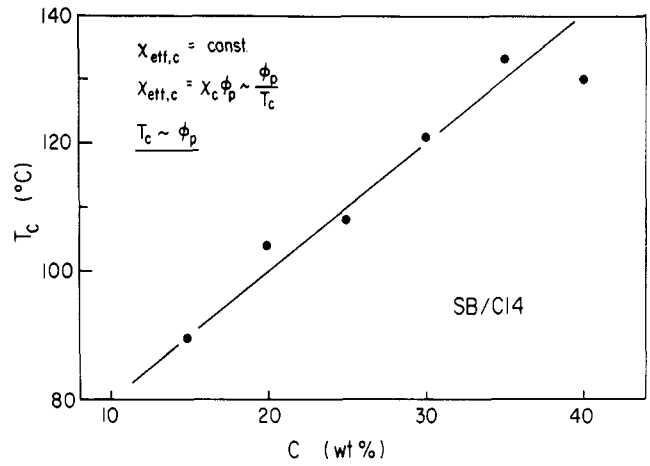

Figure 5. Estimated order–disorder transition temperature T_r as a function of polymer concentration c. T_c in the figure corresponds to T_r in the text.

Figure 5 shows the concentration dependence of the transition temperature T_r thus estimated (see also Table I). The temperature T_r is shown to increase approximately linearly with polymer concentration c. In the next section we study the kinetics of the transition after a T jump from room temperature to above T_r.

V. Kinetics of the Order–Disorder Transition

Figure 6 presents typical results on the time-resolved SAXS experiments on the order–disorder transitions after a T jump from 25 °C to the measuring temperatures of (a) T_m = 150, (b) 160, and (c) 170 °C for a 40 wt % solution of SB in C14 (T_r = 125 ± 5 °C). The results were obtained with the repetitive T-jump method using 10 repetitions (R = 10) and a time slice of 2 s (t_p = 2 s). The isometric displays qualitatively show that the decay of the scattering intensity is faster at higher T_m.

Figure 7 presents quantitatively the decay of scattered intensity at q = 0.160 nm^{-1} ($\simeq q_{max}$) with time after a T jump to 150, 160, and 170 °C for a 40 wt % SB solution in C14. The intensity decay with time is initially nonexponential but becomes exponential at a time scale much larger than τ, the retardation time required to achieve T_m by the T-jump method. The initial nonexponential behavior was found to be attributed to the finite time required for the T jump, and the observed decay behavior shown by open circles was predicted in terms of the multistep T-jump process as discussed in detail in the previous paper.[8] The solid lines are the predicted and best-fit results obtained by using the measured value of τ = 6 s and by adjusting two parameters D_0 and ΔH_a, where

$$D_{eff}(T) = D_0 \exp(-\Delta H_a/RT) \tag{22}$$

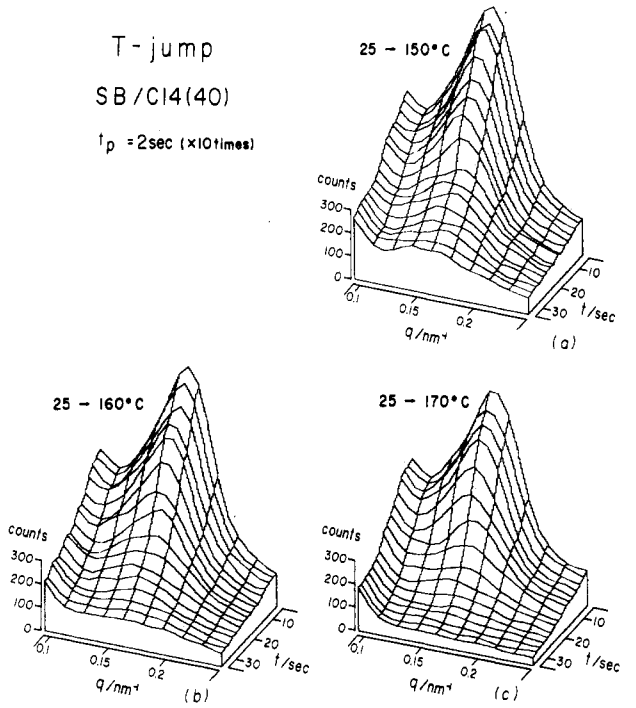

Figure 6. Isometric displays of variations of the SAXS profiles with time during the order–disorder transition. (a) to (c) corresponds to the microphase-dissolution process at 150, 160, and 170 °C, respectively. The real-time experiments were carried out with the repetitive T-jump method and the time-slice data acquisition technique as described in the text (preset time t_p = 2 s; number of repetitions R = 10).

Table II
Comparisons of the D_{eff} Values Estimated by Simulation of the Entire Intensity Decay Behavior with the Multistep T-Jump Process (Calcd) and Those Estimated from the Slope of ln $[I(q,t)/I(q,t=0)]$ vs. t at the Late Stage of the Transition (Obsd) for a 40 wt % Solution of SB in C14

	D_{eff}/(nm^2 s^{-1})	
temp, °C	calcd[a]	obsd[b]
150	1.8 ± 0.1	1.6 ± 0.05
160	2.2 ± 0.1	2.0 ± 0.1
170	3.0 ± 0.1	2.8 ± 0.1

[a] ΔH_a = 9.0 kcal/mol. [b] ΔH_a = 8.9 kcal/mol.

ΔH_a is the activation energy for the effective diffusivity. The temperature dependence of D_{eff} and ΔH_a thus estimated is summarized in Table II (see $D_{eff,calcd}$).

It was also found in the previous paper[8] that at $t \gg \tau$ the T-jump process becomes ideal, giving rise to the exponential intensity decay with time as shown by the broken straight lines in Figure 7. The slope of the straight line also yields the value D_{eff}

$$D_{eff} = |\text{slope of ln } [I(q,t)/I(q,t=0)] \text{ vs. } t|/(2q^2) \quad (\text{for } t > \tau) \tag{23}$$

The temperature dependence of D_{eff} and ΔH_a thus estimated is also summarized in Table II (see $D_{eff,obsd}$). A satisfactory agreement was obtained between the two sets of results, and hence the rest of the results were determined by using eq 23.

Figure 8 shows the measured intensity decays at various temperatures above T_τ for (a) 20, (b) 25, and (c) 30 wt % SB solutions in C14. Trends similar to those for the 40 wt % solutions were observed. The decay rate is found to increase with increasing temperature and decreasing concentration. Temperature and concentration dependencies of the effective diffusivity of the SB/C14 systems are summarized in Figures 9 and 10 and Table III.

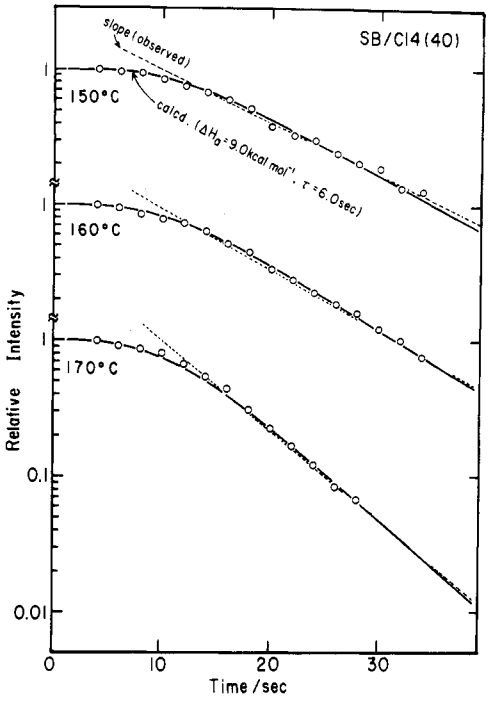

Figure 7. Decay of scattered intensity at q = 0.160 nm^{-1} (near q_{max}) with time during the microphase-dissolution processes of 40 wt % SB/C14 solutions at 150, 160, and 170 °C. The open circles represent the data points, and the solid curves are those which are best fit with the experimental results on the basis of the multistep T-jump process as described in the text. The best fits yielded an activation energy ΔH_a = 9.0 kcal/mol for the center-of-mass diffusion and the effective diffusivity ($D_{eff,calcd}$) as shown in Table II. The broken lines indicate the exponential decay of the scattered intensity at the time scale $t > \tau$, the slope of which also yields D_{eff} ($D_{eff,obsd}$) as shown in Table II.

Table III
Estimated Effective Diffusivities D_{eff} (nm^2/s) as a Function of Polymer Concentration and Temperature for the SB/C14 Solutions

	polymer concn, wt %				
temp, °C	20	25	30	35	40
110	1.5				
115	1.8				
120		1.5			
125	3.0	1.6			
130		2.3			
135	3.8	2.6			
140		2.9		1.7	
145	5.2	4.0	2.6	1.9	
150		4.4	2.9	2.1	1.6
155			3.1	2.3	
160			3.2	2.7	2.0
165			3.1	3.2	
170			5.2	3.4	2.7
175				3.5	

Figure 9 presents logarithms of the effective diffusivity as a function of $1/T$ for the polymer solutions with various concentrations. The temperature dependence of the diffusivity is found to be approximated by an Arrhenius equation (eq 22) with an activation energy ΔH_a between 9 and 12 kcal/mol. The activation energies for 20, 25, 30, 35, and 40 wt % solutions were 11, 12, 10, 8.6, and 8.9 kcal/mol.

The concentration dependence of the effective diffusivity is summarized in the plot shown in Figure 10, where the logarithms of the relative diffusivity D_{eff}/D_{eff}(35 wt %) at a given concentration c and temperature to the diffusivity

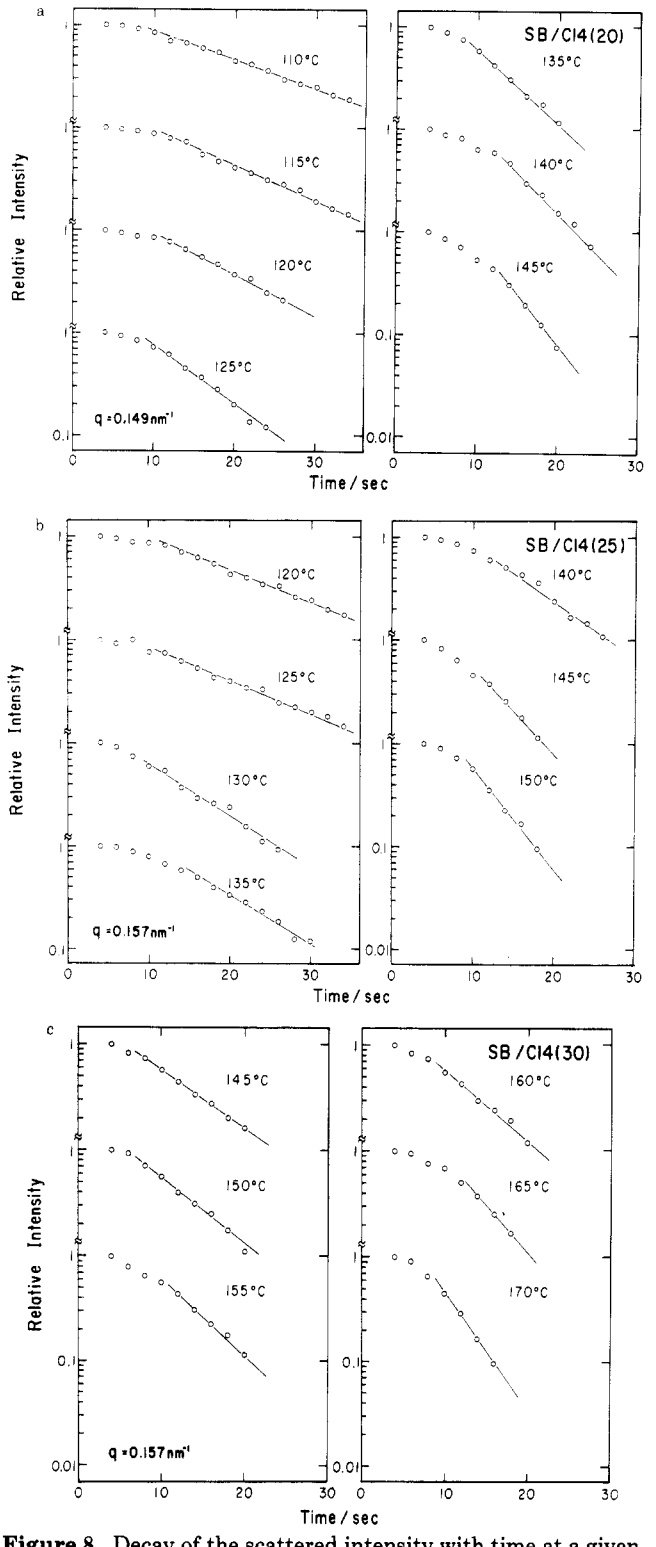

Figure 8. Decay of the scattered intensity with time at a given q and at various temperatures above T_r during the order–disorder transition for (a) 20, (b) 25, and (c) 30 wt % SB/C14 solutions.

at 35 wt % solution and at the same temperature are plotted as a function of logarithms of the given concentration relative to 35 wt % concentration $c/c(35\text{ wt }\%)$. The data points come close to the straight line with a slope of −1.75

$$D_{\text{eff}} \sim c^{-1.75} \tag{24}$$

It is quite surprising that the estimated diffusivity follows closely the scaling prediction for the semidilute solution[4] even at the high concentration range covered in this experiment. At concentrations greater than the critical concentration c^{**}, the concentration blob size becomes equal to or less than the temperature blob size, and hence the polymers are expected to reach a Θ state both globally and locally.[4] Under this condition, the effective diffusivity should obey the following scaling rule:

$$D_{\text{eff}} \sim c^{-3} \qquad \text{for } c > c^{**} \tag{25}$$

Now, c^{**} is proportional to the reduced temperature

$$\tau = (T - \Theta)/\Theta \tag{26}$$

where Θ is the theta temperature. Consequently further verification of the observed result as shown in eq 24 may deserve the assessment of the c^{**} value for SB in C14 in temperature range from 140 to 160 °C.[20]

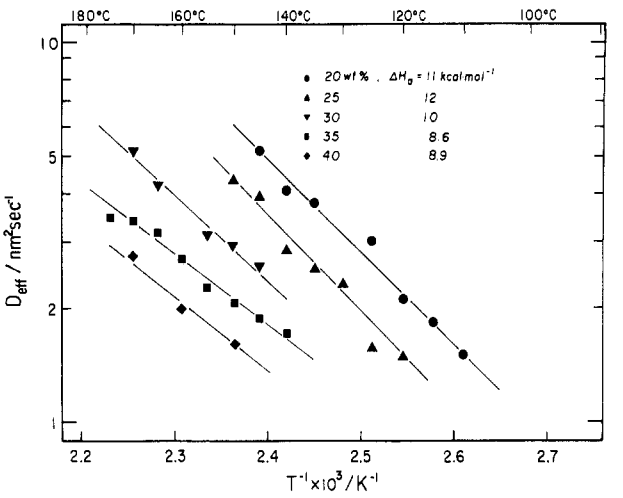

Figure 9. Estimated effective diffusivities D_{eff} as a function of $1/T$ for SB/C14 solutions with various concentrations.

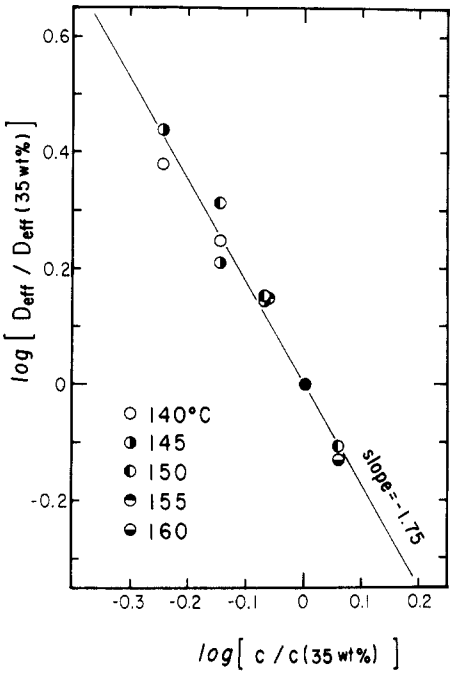

Figure 10. Concentration dependence of the effective diffusivity D_{eff}. The diffusivity for a given concentration and at a given temperature relative to that for 35 wt % solution at the same temperature is plotted against the given concentration relative to 35 wt % concentration on a logarithmic scale.

VI. Rheological Behavior

The rheological behavior of the solutions was also studied in the same temperature and concentration ranges as those where the time-resolved SAXS studies were car-

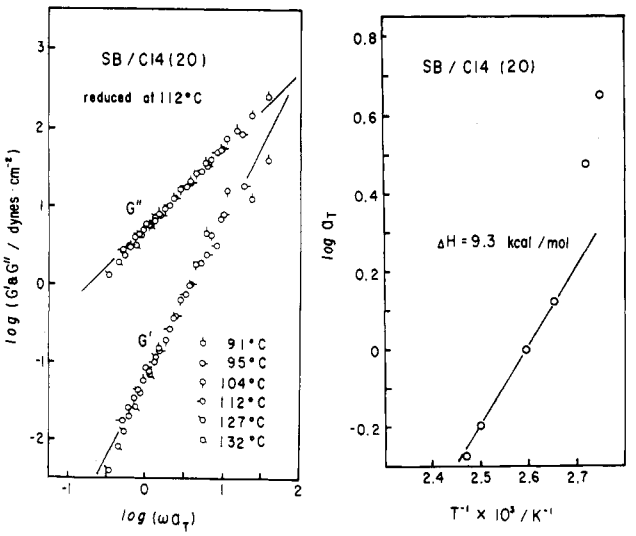

Figure 11. Master curves of the real and imaginary parts of the shear moduli G' and G'' reduced at 112 °C and the temperature dependence of the shift factor a_T for a 20 wt % SB/C14 solution.

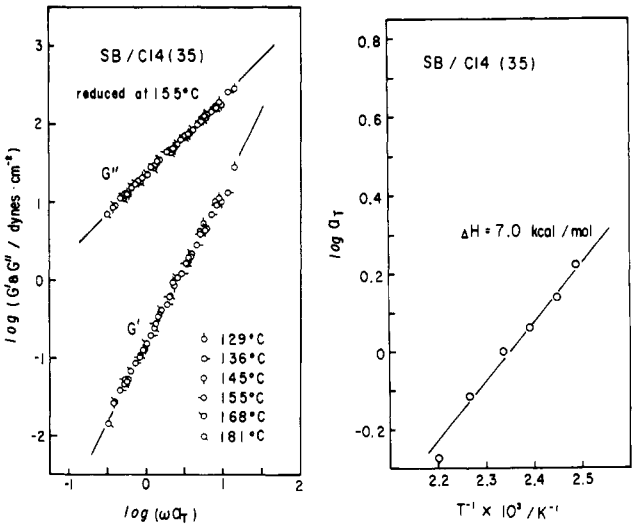

Figure 12. Master curves of the real and imaginary parts of the shear moduli G' and G'' reduced at 155 °C and the temperature dependence of the shift factor a_T for a 35 wt % SB/C14 solution.

ried out. Typical results are shown in Figures 11 and 12 for 20 and 35 wt % polymer solutions, respectively. Figures 11 and 12 present the master curves of G' and G'' with the reduced frequency ωa_T and the temperature dependence of the shift factor a_T.

For the 20 wt % polymer solution, T_r was estimated to be 95 °C. It is clearly seen that the data at temperatures higher than T_r smoothly fall onto the master curves and show Newtonian flow behavior, G' and G'' having slopes of 2 and 1 in the plots. The activation energy for the flow process is estimated to be 9.3 kcal/mol, which is close to the value (11 kcal/mol) estimated from the time-resolved SAXS technique in the similar temperature range. The data points at 91 and 95 °C tend to deviate from the master curves, and the corresponding activation energies also show deviation from the values extrapolated from the activation energies at higher temperatures. These deviations are a result of the difference of the flow mechanism at the higher and lower temperatures. The non-Newtonian flow behavior at the lower temperatures is attributable to the existence of microdomains and reflects the flow in the ordered state.

All the data points for 35 wt % polymer solutions (Figure 12) were obtained at temperatures above T_r and reflect the flow behavior in the disordered state. Consequently all the data points smoothly fall onto the master curves, and the solution exhibits Newtonian flow behavior with an activation energy $\Delta H_a = 7.0$ kcal/mol. The energy is again close to that measured by the SAXS technique in the same temperature range (8.6 kcal/mol). Consequently both the SAXS intensity decay behavior and the rheological behavior reflect a common physical process, i.e., translational diffusion of the center of mass of block polymer solutions at $T > T_r$.

It should be noted that the concentration dependence of G' and G'' as shown in Figures 11 and 12 seems to follow approximately the scaling predictions for semidilute solutions;[4,11,16,17] the data on G'' at the two different concentrations in the flow region can be approximately superposed by plotting G'/G_N° as a function of $\omega\tau_m$, with the following scaling rules:

$$G_N^\circ \sim c^{2.25} \tag{27}$$

$$\tau_m \sim c^2 \tag{28}$$

where G_N° is the quasi-equilibrium shear modulus (the plateau modulus) and τ_m is the disengagement time of the polymer chains from the tube. This observation is consistent with the observation leading to eq 24.

Acknowledgment. We express our sincere thanks to Professor T. Kotaka and Dr. H. Watanabe for the rheology measurements which led to the results shown in Figures 11 and 12 and also for stimulating discussions.

Appendix: Derivation of Eq 5 for a Polymer Mixture

In order to gain some insight into the physical meaning of D_{eff} in eq 5, especially the effect of thermodynamic interaction χ between polymers A and B on $\rho_K(\mathbf{r},t)$, we consider here an analogous problem in the polymer mixtures (rather than the block polymer systems). Let us consider dissolution of initially existing segmental density fluctuations $\rho_K(\mathbf{r},t)$ in the polymer mixture composed of polymers A and B. The dissolution is induced thermodynamically by bringing the mixture in the single-phase region.

The decay of the concentration fluctuation of a K segment with time is given by the continuity equation

$$-\frac{\partial \rho_K(\mathbf{r},t)}{\partial t} = \text{div } \mathbf{J}_K \qquad (K = A, B) \tag{A-1}$$

where $\mathbf{J}_K$ is the diffusional flux generated by gradients of chemical potentials $\nabla\mu_K$

$$\mathbf{J}_A = -\frac{\Lambda}{k_B T}\nabla(\mu_A - \mu_B) \tag{A-2}$$

and Λ is the Onsager coefficient. Equation A-2 was obtained under the assumption of incompressibility

$$\mathbf{J}_A + \mathbf{J}_B = 0 \tag{A-3}$$

and by using Onsager's reciprocal relation

$$\Lambda_{AB} = \Lambda_{BA} \tag{A-4}$$

in eq A-2 as defined as

$$\Lambda = \Lambda_{AA} = \Lambda_{BB} = -\Lambda_{AB} = -\Lambda_{BA} \tag{A-5}$$

Now the chemical potential difference $(\mu_A - \mu_B)$ may be calculated on the basis of the Flory–Huggins lattice model. The free energy per lattice site F is given by

$$F/k_B T = [\rho_A \ln \rho_A + \rho_B \ln \rho_B]/N + \chi\rho_A\rho_B \tag{A-6}$$

Here it was assumed, to simplify arguments, that the A

and B polymers have the same degree of polymerization

$$N_A = N_B = N \tag{A-7}$$

From eq A-6, one obtains

$$\frac{\mu_A - \mu_B}{k_B T} = \frac{\partial(F/k_B T)}{\partial \rho_A} = \frac{1}{N} \ln\left(\frac{\rho_A}{\rho_B}\right) + \chi(1 - 2\rho_A) \tag{A-8}$$

In eq A-6 and A-8, the nonlocal energetic and entropic interactions (such as the term related to the gradient free energies $\kappa(\nabla\rho_K)^2$) were neglected. Taking the gradient on both sides of eq A-8, one obtains

$$\frac{\nabla^2(\mu_A - \mu_B)}{k_B T} = \left[\frac{1}{N\rho_A\rho_B} - 2\chi\right]\nabla^2\rho_A + \text{nonlinear terms} \tag{A-9}$$

From eq A-1, A-2, and A-9, the q Fourier component of the fluctuation $\rho_K(q,t)$ is given by

$$\frac{1}{\rho_K(q,t)}\frac{\partial\rho_K(q,t)}{\partial t} = -q^2\Lambda\left[\frac{1}{N\rho_A\rho_B} - 2\chi\right]\rho_K(q,t) \tag{A-10}$$

In obtaining eq A-10, the nonlinear terms in eq A-9 were neglected and the following relationship was used:

$$\nabla^2\rho_K(q,t) = -q^2\rho_K(q,t) \tag{A-11}$$

In the small-q regime satisfying $qR_0 \ll 1$, where R_0 is the individual polymer coil dimension in the mixture, de Gennes' scaling arguments give

$$\Lambda = N\rho_A\rho_B D_c \tag{A-12}$$

where D_c is the diffusivity of polymers A and B, which are assumed to be identical. From eq A-10 and A-12, it follows that

$$\rho_K(q,t) = \rho_K(q,0)\exp[-R(q)t] \tag{A-13}$$

$$R(q) = q^2 D_c(\chi_s - \chi)/\chi_s \equiv q^2 D_{eff} \tag{A-14}$$

and

$$\chi_s = [2N\rho_A\rho_B]^{-1} \tag{A-15}$$

where χ_s is the χ value at the spinodal point. Thus it is obvious that D_{eff} is a function of thermodynamic interaction $(\chi_s - \chi)/\chi_s$ and of frictional interaction D_c. The exponential decay of the segmental density fluctuations with time as given by eq A-13 predicts also the exponential decay of the scattered intensity $I(q,t)$

$$I(q,t) = I(q,t=0)\exp[-2R(q)t] \tag{A-16}$$

On the basis of the hypothesis that a similar argument may be applied to the block polymer problem, we can have an insight into the physical factors influencing the mutual diffusion coefficient D_{eff}. However, it is needless to say that the problem is more complicated for block polymers than for polymer blends due to the effects of connectivity between A and B in A–B diblock polymers. The problem in the block polymer is essentially unsolved and deserves future investigation.

References and Notes

(1) Leibler, L. *Macromolecules* **1980**, *13*, 1602.
(2) Hashimoto, T.; Shibayama, M.; Kawai, H. *Macromolecules* **1983**, *16*, 1093.
(3) Mori, K.; Hasegawa, H.; Hashimoto, T. *Polym. J.* **1985**, *17*, 799.
(4) de Gennes, P.-G. "Scaling Concepts in Polymer Physics"; Cornell University Press: Ithaca, NY, 1979.
(5) LeGrand, A. D.; LeGrand, D. G. *Macromolecules* **1979**, *12*, 450.
(6) Leibler, L.; Benoit, H. *Polymer* **1981**, *22*, 195.
(7) Benmouna, M.; Benoit, H. *J. Polym. Sci., Polym. Phys. Ed.* **1983**, *21*, 1227.
(8) Hashimoto, T.; Kowsaka, K.; Shibayama, M.; Suehiro, S. *Macromolecules* **1986**, *19*, 750.
(9) Hashimoto, T.; Tsukahara, Y.; Kawai, H. *Macromolecules* **1981**, *14*, 708.
(10) de Gennes, P.-G. *J. Chem. Phys.* **1971**, *55*, 572.
(11) Doi, M.; Edwards, S. F. *J. Chem. Soc., Faraday Trans. 2* **1978**, *74*, 1789, 1802, 1818.
(12) Hosemann, R.; Bagchi, S. N. "Direct Analysis of Diffraction by Matter"; North-Holland Publishing Co.: Amsterdam, 1962.
(13) Shibayama, M.; Hashimoto, T.; Kawai, H. *Macromolecules* **1983**, *16*, 16.
(14) Hashimoto, T.; Shibayama, M.; Kawai, H.; Watanabe, H.; Kotaka, T. *Macromolecules* **1983**, *16*, 361.
(15) Upon extending Leibler's theory for bulk block polymers[1] to concentrated block polymer solutions, Hashimoto et al. erroneously replaced the intensity I in eq 15 by I/ϕ_p^2 (see eq IV-12 of ref 2). The intensity I in eq 15 should be rather replaced by I/ϕ_p. Thus

$$(I/\phi_p)^{-1} \sim (F(u')/N - \chi\phi_p)$$

or

$$I^{-1} \sim (F(u')/N\phi_p - \chi)$$

(16) Raju, V. R.; Menezes, E. V.; Marin, G.; Graessley, W. W.; Fetters, L. J. *Macromolecules* **1981**, *14*, 1668.
(17) Takahashi, M.; Masuda, T. *Rep. Prog. Polym. Phys. Jpn.* **1984**, *27*, 145.
(18) Hashimoto, T.; Nagatoshi, K.; Todo, A.; Hasegawa, H.; Kawai, H. *Macromolecules* **1974**, *7*, 364.
(19) See, for example: Shibayama, M.; Hashimoto, T. *Macromolecules* **1986**, *19*, 740.
(20) It should be further noted that the scaling law on D_{eff} of the block polymer involves the thermodynamic interaction as demonstrated by the factor $(\chi_s - \chi)/\chi_s$ in the Appendix (eq A-14) as well as the diffusivity D_c as in the corresponding scaling law for homogeneous systems. The complication associated with $D_{eff}(\chi)$ should be clarified in the future. However, it is qualitatively expected that the observation of the scaling law as given by eq 24 may be a consequence of the observations under a constant thermodynamic driving force, $[\chi_s(c) - \chi(c, T)]/\chi_s(c)$.